

Superfluids in rotation: Landau-Lifshitz vortex sheets vs Onsager-Feynman vortices

G.E. Volovik^{1,2}

¹Low Temperature Laboratory, Aalto University, P.O. Box 15100, FI-00076 AALTO, Finland

²L. D. Landau Institute for Theoretical Physics, 117940 Moscow, Russia

(Dated: May 26, 2022)

The paper by Landau and Lifshitz on vortex sheets in rotating superfluid appeared in 1955 almost at the same time when Feynman published his paper on quantized vortices in superfluid ^4He . For a long time this paper has been considered as an error. But 40 years later the vortex sheets have been detected in chiral superfluid $^3\text{He-A}$ in the rotating cryostat constructed in the Olli Lounasmaa Low Temperature Laboratory (Otaniemi, Finland). The equation derived by Landau and Lifshitz for the distance between the vortex sheets as a function of the angular velocity of rotation has been experimentally confirmed, which is the triumph of the theory. We discuss different configurations of the vortex sheets observed and to be observed in superfluid $^3\text{He-A}$.

PACS numbers:

I. INTRODUCTION: QUANTIZED VORTICES AND VORTEX SHEET

Superfluid liquids were believed to obey the irrotational (potential) flow, $\nabla \times \mathbf{v}_s = 0$. However, experiments by Andronikashvili and Osborne demonstrated formation of meniscus in superfluid ^4He under rotation. This indicated that this superfluid rotates as a normal liquid, i.e. it participates in the solid body rotation, $\mathbf{v}_s = \boldsymbol{\Omega} \times \mathbf{r}$ and thus $\nabla \times \mathbf{v}_s = 2\boldsymbol{\Omega}$. To resolve this puzzle two scenarios were suggested in 1955: by Feynman¹ and by Landau and Lifshitz². In the Feynman approach the solid body rotation on a macroscopic scale is imitated by the array of quantized vortices in Fig. 2 (*top left*).

Landau and Lifshitz had another idea. They suggested that irrotational circulating flow was concentrated between the cylindrical vortex sheets (Fig. 1 *top right*). Historically, vorticity concentrated in sheets was suggested by Onsager in 1948^{3,4}. In this arrangement the

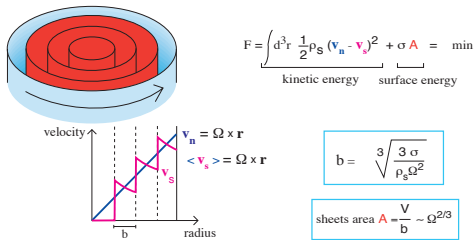


FIG. 1: Vortex sheet scenario by Landau and Lifshitz (1955). Due to cylindrical vortex sheets the potential flow of superfluid component between the sheets simulates the solid body rotation of liquid in average. The distance b between sheets as function of angular velocity Ω of rotation is found by minimization of kinetic energy of flow and surface tension of the tangential discontinuity.

vortex sheet is unstable in superfluid ^4He towards vortex lines

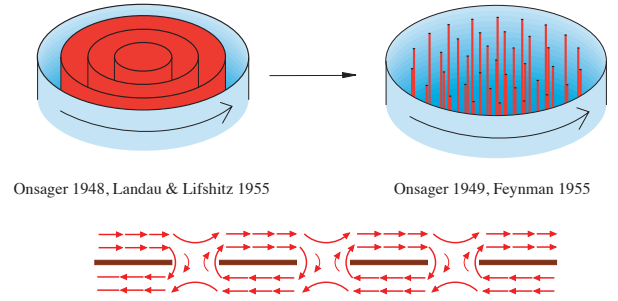


FIG. 2: Vortex sheet is unstable in superfluid ^4He towards vortex lines.

flow of superfluid component also corresponds to the solid body rotation on a macroscopic scale (Fig. 1 *bottom left*). By the minimization of energy Landau and Lifshitz calculated the spacing b between the neighboring vortex sheets:

$$b = \left(\frac{3\sigma}{\rho_s \Omega^2} \right)^{1/3}. \quad (1)$$

It is determined by the balance of the kinetic energy of the superflow in rotating frame, $\frac{1}{2}\rho_s(\mathbf{v}_s - \mathbf{v}_n)^2$, and the surface tension σ of the sheets (Fig. 1 *right*).

The surface tension of the tangential discontinuity in superfluid ^4He has been estimated by Ginzburg⁵, and the effective density of the rotating superfluids with vortex sheets has been calculated by I.M. Lifshitz and M.I. Kaganov.⁶

II. VORTEX SHEET INSTABILITY IN SUPERFLUID ^4He

It turned out, however, that in superfluid ^4He the vortex sheet scenario does not work for several reasons. First, the tangential discontinuity is unstable towards break-up of the sheet into separate pieces (Fig. 2 *bottom*), which finally transform to the quantized vortex lines in Fig. 2 (*top left*).

Then, there is the nucleation problem. According to Landau and Lifshitz the system of the equidistant layers should exist at sufficiently high velocity Ω of rotation. At low Ω a small cylindrical sheet appears first. As we know now the objects are not easily created in the bulk liquid: they appear on the boundary and then propagate to the bulk. This would mean that with increasing angular velocity, the elementary cylindrical sheets start to penetrate into rotating vessel. Moreover, at high velocity the array of small sheets is energetically more favorable than the system of the coaxial sheets. All this suggests, that the scenario of the coaxial vortex sheets may never occur.

Nevertheless, though the Landau-Lifshitz scenario was not applicable to the trivial superfluidity in liquid ^4He , this idea turned out to be exactly to the point for chiral superfluid $^3\text{He-A}$. First, the vortex sheet there is locally stable, being based on topological soliton. Second, the sheet is formed from the boundary of container. And finally, though the system of small cylinders and the system of quantized vortices are energetically more favorable, they are not formed in the process of the growth of the vortex sheet state.

The Landau-Lifshitz equation (1) for distance between the vortex sheets as a function of Ω has been experimentally confirmed in the NMR measurements, which was the triumph of the theory. The Bragg reflection from the locally equidistant sheet planes has been also found⁷.

III. CONTINUOUS VORTICITY IN CHIRAL SUPERFLUID $^3\text{He-A}$: SKYRMIONS AND MERONS

The chiral superfluid $^3\text{He-A}$ is an orbital ferromagnet with magnetization along the orbital angular momentum $\hat{\mathbf{l}}$ of Cooper pair⁸. Simultaneously it is the spin antiferromagnetic (spin nematic) with anisotropy axis $\hat{\mathbf{d}}$, which allows us to investigate the properties of $^3\text{He-A}$ using NMR.

The typical vortices, which appear in the chiral superfluid $^3\text{He-A}$ under rotation, are continuous vortices – textures without singularity in the order parameter field, Fig. 3 (*left*). The structure of the $\hat{\mathbf{l}}$ -field in the continuous vortex is similar to the structure of skyrmions – the topologically twisted continuous field configurations in quantum field theory⁹. The topological winding number of the skyrmion texture gives rise to the quantized circulation of superfluid velocity around the skyrmion¹⁰.

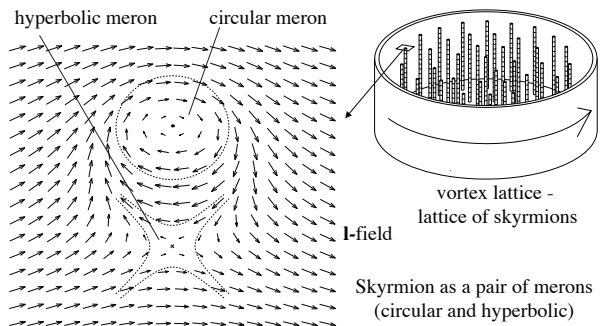


FIG. 3: Superfluid $^3\text{He-A}$ is orbital ferromagnet with magnetization along the orbital angular momentum $\hat{\mathbf{l}}$ of Cooper pair, and spin antiferromagnetic (spin nematic) with anisotropy axis $\hat{\mathbf{d}}$. Typical vortices, which are created in $^3\text{He-A}$ under rotation, are continuous vortices with 4π winding of the condensate phase around the vortex (two quanta of circulation). The vorticity is generated by texture in the ferromagnetic field $\hat{\mathbf{l}}$, which is called the skyrmion. Skyrmion can be represented as the bound state of two merons, circular and hyperbolic. Each meron represents a vortex with a single quantum of circulation (the so-called Mermin-Ho vortex¹⁰). In the circular vortex-meron $\hat{\mathbf{l}} \parallel \Omega$ in the center, while in the hyperbolic vortex-meron $\hat{\mathbf{l}} \parallel -\Omega$ in the center.

Skyrmion represents the vortex with two quanta of circulation ($N = 2$), i.e. the phase of the order parameter changes by 4π , when circling around the vortex.

Skyrmion consists of two radicals, called merons, each with the circulation number $N = 1$ (the 2π -vortex). The isolated meron cannot exist in the bulk liquid for topological reasons. Vortex-skyrmions have been experimentally identified in $^3\text{He-A}$ in NMR experiments¹¹. The lattice of skyrmions has been later discovered also in magnetic materials¹².

IV. SOLITONS AND MERONS

The other possibility of existence of merons is within the core of the topological soliton. Topological $\hat{\mathbf{l}}$ -soliton in superfluid $^3\text{He-A}$ in Fig. 4 (*top*) looks similar to the Bloch or Neel wall in ferromagnets. However, its topology is different: it is characterized by the nontrivial element of Z_2 relative homotopy group. Meron appears there in the form of a kink in the $\hat{\mathbf{l}}$ -soliton, Fig. 4 (*bottom*). The kink separates two parts of the same soliton, which have the opposite parities. The solitonic meron looks similar to the Bloch line within the Bloch wall in ferromagnets¹⁵, and it also cannot escape from the soliton (domain) wall.

For us it is important that merons carry the quantum of vorticity, $N = 1$, and thus they serve as the building

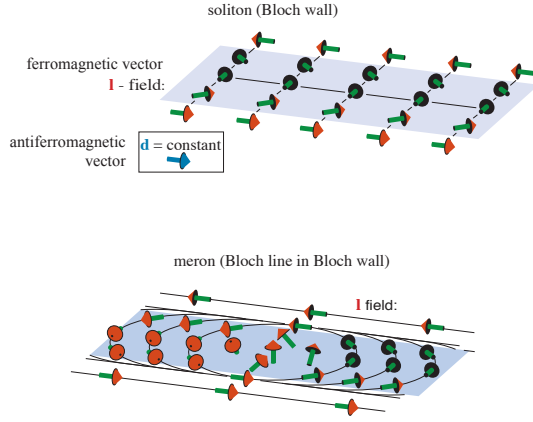


FIG. 4: *top*: Topological soliton in superfluid $^3\text{He-A}$ is the analog of the Bloch or Neel wall in ferromagnets. It is characterized by the nontrivial element of Z_2 relative homotopy group. Figure demonstrates the $\hat{\mathbf{l}}$ -soliton, in which the ferromagnetic vector $\hat{\mathbf{l}}$ changes the direction to the opposite, while the antiferromagnetic vector $\hat{\mathbf{d}}$ remains constant. As distinct from the domain wall, the soliton can terminate on a singular topological defect – the vortex with π winding number ($N = 1/2$, the half-quantum vortex^{13,14}), see Fig. 11. *bottom*: Bloch line within Bloch wall represents meron, which is the 2π vortex ($N = 1$).

blocks for construction of the vortex sheets, which are experimentally investigated in superfluid $^3\text{He-A}$ ^{7,16,17}.

V. VORTEX SHEET AS A CHAIN OF MERONS

When the topologically stable soliton accumulates vorticity in the form of merons with the same circulation number $N = 1$, it forms the vortex sheet, Fig.5 (*top right*). The vortex sheet has a hierarchy of length scales^{18,19}. On a macroscopic scale the planes of the vortex sheets have a local order of the smectic liquid crystal, Fig.5 (*top left*). The neighbouring planes of the vortex sheet are separated by layers with the vortex-free superflow, Fig.5 (*bottom left*).

According to Landau-Lifshitz theory, the vortex sheets allow for the solid-body like rotation of the superfluid on a macroscopic scale, i.e. with the average velocity field obeying equation $\langle \mathbf{v}_s \rangle = \boldsymbol{\Omega} \times \mathbf{r}$, and thus $\langle \nabla \times \mathbf{v}_s \rangle = 2\boldsymbol{\Omega}$.

VI. GROWTH OF THE FOLDED VORTEX SHEET. THEORY

Numerical simulation of the growth of the vortex sheet¹⁸ is shown in Fig. 6. It follows from the experimental observations that once the vortex sheet appears in the cell, the critical velocity of entering new merons into the cell is essentially smaller than the critical velocity of the formation of skyrmions (about 6-7 times

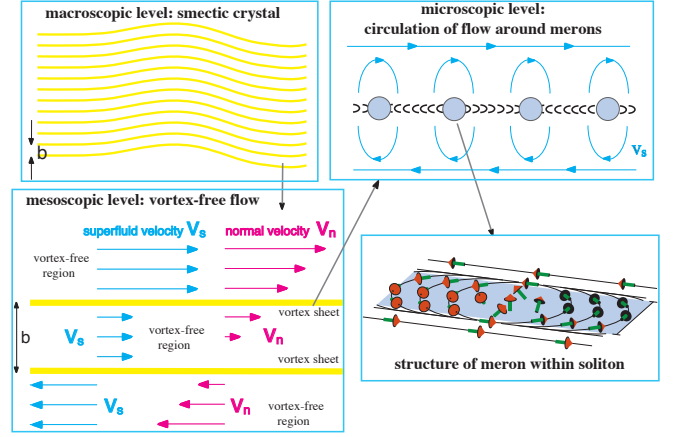


FIG. 5: Vortex sheet structure. (*top left*): On macroscopic scale the planes of the vortex sheets form a local order of the smectic liquid crystal. (*bottom left*): Flow velocity fields of superfluid and normal components between the sheet planes. In these regions the superflow is vortex-free (superfluid velocity is constant), while the velocity of the normal component $\mathbf{v}_n = 2\Omega y \hat{\mathbf{x}}$ with $\nabla \times \mathbf{v}_n = 2\boldsymbol{\Omega}$. (*top right*): Flow velocity field of superfluid component around merons (Mermin-Ho $N = 1$ vortices). (*bottom right*): Structure of an individual circular meron.

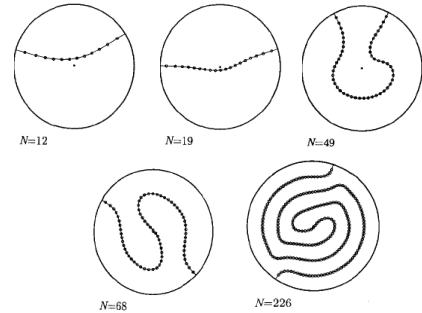


FIG. 6: Numerical simulation of the growth of the vortex sheet with adiabatically increasing angular velocity of rotation Ω . N is the number of merons in sheet. Vortex sheet is formed in the rotating vessel, if the topological soliton is present in the cell. With increasing Ω , merons enter the soliton from the side wall, and the folded vortex sheet is formed. For large Ω the configuration approaches that of the Landau-Lifshitz cylindrical vortex sheets, but these sheets are connected. The dependence of the number of vortex-merons $N(\Omega)$ on angular velocity approaches the function $N_0(\Omega) = (2m/\hbar)\Omega R^2$, which does not depend on the surface tension of the soliton and corresponds to the equilibrium number of the isolated vortices in the rotating container. In the range $12 < N < 19$ the vortex sheet has the form of the plane along the diameter of the cylinder, see Fig. 7.

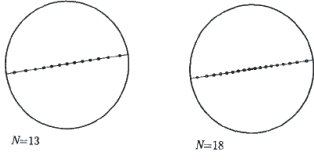


FIG. 7: Straight vortex sheet is formed in the interval $12 < N < 19$. The meron number $N(\Omega)$ in this configuration does not depend on the soliton tension, since its area of the soliton does not change within this interval. Eq.(4) gives $N(\Omega) = 0.42N_0(\Omega)$.

less). Merons have a small critical velocity for creation because the soliton is always in a close contact with the side wall. The new merons are created at the edges of the soliton at the wall and then easily enter the soliton. That is why the further acceleration of the angular velocity leads to the growth of the soliton rather than to the creation of new skyrmions. In the final state of such adiabatic growth the skyrmions are absent, while the multiply folded vortex sheet is formed, which locally simulates the coaxial sheets of Landau-Lifshitz, see Fig. 6 (*bottom right*). Note that in this figure the maximal number of merons was $N = 226$, while in experiments N can reach 10^3 , where the coaxial cylindrical structure of the folded vortex sheet is more pronounced.

The number of merons in the vortex sheet depends on angular velocity Ω of the rotating vessel. For large Ω the number of vortices-merons $N(\Omega)$ in the cell approaches the value $N_0(\Omega) = (2m/\hbar)\Omega R^2$, where m is the mass of the ^3He atom. This function $N_0(\Omega)$ does not depend on the surface tension of the soliton, it corresponds to the solid body rotation of the superfluid component, $\langle \nabla \times \mathbf{v}_s \rangle = 2\Omega$.

VII. PLANAR VORTEX SHEET

For small Ω the finite size is present: surface tension of the soliton becomes important, and as a result the meron number is smaller than that which corresponds to the macroscopic solid body rotation of the liquid, $N(\Omega) < N_0(\Omega)$. Note that the vortex sheet itself performs the solid body rotation together with the container, but the flow of the whole liquid does not follow the solid body rotation. The same deficit of the effective density of the liquid involved into rotation has been considered by

I.M. Lifshitz and M.I. Kaganov⁶ for the Landau-Lifshitz concentric sheets.

In our case of the vortex sheet connected to the side walls of container, the shape of sheet depends on angular velocity Ω and thus on the number N of merons. There is the range of velocities, where the equilibrium configuration of the vortex sheet is the straight soliton along the diameter of the cylinder (the plane which contains the axis of cylinder). In Fig. 6 this is the range $12 < N < 19$. For the straight soliton the function $N(\Omega)$ can be found analytically.

Let x be the coordinate along the straight soliton with $x = 0$ on the axis of container and $n(x)$ is the density of vortex-merons in the soliton (the 2π -vortices). If one neglects the image forces from the boundary, the equation for $n(x)$ is

$$\frac{\hbar}{2m} \int_{-R}^R dy \frac{n(y)}{x-y} = \Omega x. \quad (2)$$

This corresponds to the solid body rotation of the soliton (the soliton is stationary in the rotating frame if superflow velocity produced by other vortices at the place of a given meron is equal to the solid body velocity $v_y = \Omega x$). The soliton surface tension does not enter since the length of the soliton is always the same, $L = 2R$. The equation (2) has solution

$$\frac{\hbar}{2m} n(x) = \frac{\Omega}{\pi} \sqrt{R^2 - x^2}. \quad (3)$$

The total number of merons is $N = \int dx n(x) = N_0/2$. This should be corrected by adding the images of vortices. With vortex images, the Eq.(2) transforms to

$$\frac{\hbar}{2m} \int_{-R}^R dy n(y) \left(\frac{1}{x-y} - \frac{1}{x - \frac{R^2}{y}} \right) = \Omega x, \quad (4)$$

which gives $N \approx 0.42N_0$.

VIII. NMR SIGNATURE OF THE VORTEX SHEET

The properties of different textures in $^3\text{He-A}$ (solitons, vortices and vortex sheets) are investigated using NMR, see e.g. review papers^{19,20}. The cores of these topological objects produce the potential wells for the spin wave (magnons) in Fig. 8 (*top left*). Excitation of magnons in the bound state gives rise to the satellite peak in the NMR absorption spectrum at the frequency below the main peak. The position of the satellite peak indicates the type of the object, while the intensity of the peak gives the information on the size of the object or on the number of the identical objects.

If the rotating state represents the array of vortex-skyrmions, the intensity is proportional to the number of vortices, and thus is linear in Ω , Fig. 8 (*right*). In the vortex sheet state of rotation the NMR absorption in

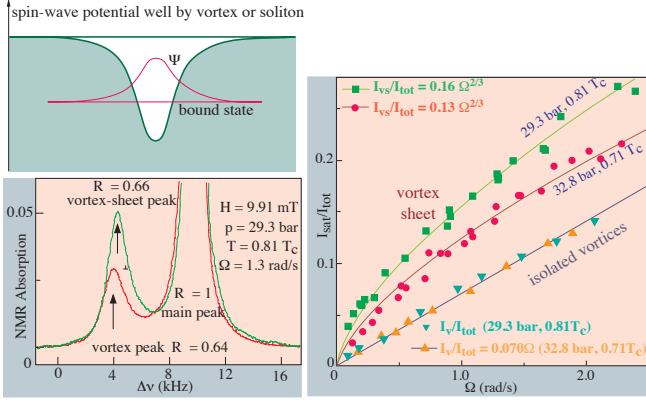


FIG. 8: NMR absorption on skyrmions and on the vortex sheet. *top left*: The core of skyrmion and the soliton represent correspondingly the 2D and 1D potential wells for spin waves – magnons. In the NMR experiments the bound states of magnons in these potentials are excited. This corresponds to the satellites in the NMR spectrum on the lower frequency side of the main peak (*bottom left*). The vortex sheet state has higher absorption than the lattice of isolated skyrmions, since the area of the soliton is larger than the area of the vortex cores. *right*: Intensity of the satellite peak as a function of the angular velocity Ω of rotation. In the vortex lattice state the intensity is proportional to the number of vortices, $N_0(\Omega) = (2m/h)\Omega R^2$, and thus is linear in Ω . In the vortex sheet state the intensity is proportional to the area of the soliton, and thus to $\Omega^{2/3}$, which agrees with the Landau-Lifshitz equation.

terms of Ω is close to the $\Omega^{2/3}$ law, Fig. 8 *right*. This is consistent with the Landau-Lifshitz equation (1). The area of the soliton is $A = V/b$, where V is the volume of the cell, and according to the Landau-Lifshitz equation one has $A \propto \Omega^{2/3}$.

In the vortex-sheet state the measured absorption is 1.5-3 times higher than in a pure vortex-skyrmion state, Fig. 8 (*bottom left*). The vortex sheet produces the potential well for magnons, which area per one quantum of circulation is larger than the area of the core of skyrmion.

IX. BRAGG PEAK AS SIGNATURE OF LAYERED STRUCTURE OF VORTEX SHEET

Locally the folded vortex state represents equidistant layers, and thus has a local order of the smectic liquid crystal (Fig. 5 *top left*). In NMR experiments such periodic structure is manifested by the Bragg peak in Fig. 9. The measured distance b between the sheets in Fig. 9 (*top left*) is in a good agreement with the Landau-Lifshitz equation (1), where the known values of the superfluid density and the soliton tension are used.

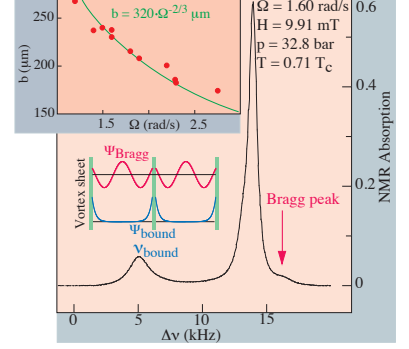


FIG. 9: (*main frame*): There is a small peak in the NMR spectrum on the higher frequency side of the main peak. It corresponds to the Bragg reflection satellite from standing spin waves between the neighbouring sheets. The experimental curve for the distance $b(\Omega)$ between the sheets (*top left*) is in agreement with the Landau-Lifshitz equation (1) within 10% accuracy.

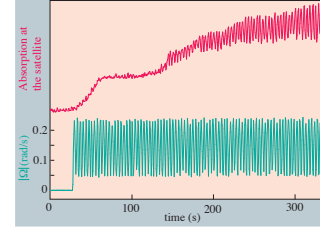


FIG. 10: Straight soliton is formed by periodic oscillation of container. The formation of this soliton is indicated by plateau in the absorption, since the area of the straight soliton does not depend on the number of merons. After the straight soliton is formed, the folded vortex sheet is obtained by adiabatic growth of the soliton by gradual increasing of the rotation velocity.

X. FORMATION OF THE VORTEX SHEET. EXPERIMENT.

In experiment, the vortex sheet is reproducibly created during the sinusoidal modulation of velocity $\Omega = \Omega_0 \sin(\omega t)$, see Fig. 10 *bottom*. The period of modulation is usually $T = 2\pi/\omega \approx 10$ s. The vortex sheet appears if the amplitude Ω_0 of modulation exceeds some critical velocity which is slightly above the critical velocity for the nucleation of the skyrmions. This means that the for-

mation of the vortex sheet is somehow connected to the presence of skyrmions in the cell. During multiple and fast alteration of the angular velocity of the container the skyrmions cannot maintain the equilibrium arrangement corresponding to a momentary angular velocity. They are pressed to the side wall of the container, where their mutual collapse supposedly gives rise to a small seed of the soliton attached to the surface of container.

Anyway, once the soliton is created, the critical velocity for entering new vorticity – merons – into the soliton from the wall is found to be essentially smaller than the critical velocity for the creation of isolated skyrmions. Thus the soliton is able to grow by absorbing the merons created at the wall. Finally the soliton with accumulated merons forms the folded vortex sheet connected with the side wall.

The upper frame of Fig. 10 displays the absorption at the satellite as a function of time. In the beginning of the modulation the increase of the absorption is small and corresponds to nucleation of few separate continuous vortices. After 2.5 minutes the first seed of the vortex-soliton is created and develops within ≈ 20 seconds to constant level, where there is no sinusoidal structure in absorption. This corresponds to the formation of the straight soliton in Fig. 7. During periodic drive the absorption remains constant, because the area of the vortex sheet does not change. The intensity of the satellite also agrees with the straight soliton. The numerical simulation shows that the straight shape of the vortex sheet is the stable configuration in the certain window of the meron number N in the soliton: $12 < N < 19$ ¹⁸.

When Ω is increased and exceeds some critical value the straight soliton becomes unstable against the curved one. At large N and Ω the length of the soliton grows and finally the folded vortex sheet sweeps all the cell to produce the homogeneous distribution of merons, which in average imitates the solid body rotation of superfluid, $\langle \mathbf{v}_s \rangle = \mathbf{\Omega} \times \mathbf{r}$. Instead of one scale, which characterizes the intervortex distance in the conventional vortex array, the vortex sheet is characterized by two scales: intervortex distance within the sheet and the mean distance b between the neighbouring parts of the curved soliton.

XI. TOPOLOGICAL STABILITY OF THE VORTEX-SHEET

The topological stability of both the soliton and the kinks (merons) inside the soliton prevents the vortex sheet from breaking into the individual vortices and thus the sheet is extended from one boundary to another. The termination of the vortex sheet in the bulk can occur only if the termination line represents the half-quantum vortex¹³. This is the object with the singular core of the coherence length size (hard core), which is the counterpart of the Alice string in high energy physics and of the object with the one-half of the magnetic flux quanta observed in high temperature superconductors¹⁴.

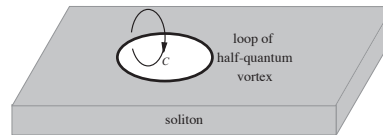


FIG. 11: Stability of the vortex sheet. Vortex sheet is based on the topological soliton. As distinct from the ferromagnetic domain walls, it is possible to drill a hole in the soliton. Such hole is bounded by the topological line defect – the string loop, where the string is the half-quantum vortex (vortex with winding number $N = 1/2$). If the vortex loop with the radius exceeding the critical value on the order of the thickness of the soliton wall ($\sim 10 \mu\text{m}$) is created, the loop will further grow and destroy the whole vortex sheet. It is known that neutron irradiation produces the hot spots (micro Big-Bang²¹) of the proper size, but all the attempts to destroy the vortex sheet by the neutron irradiation failed.

If one manages to create the loop of the half-quantum vortex within the soliton (Fig. 11) with the radius exceeding the critical value on the order of the soliton thickness ($\sim 10 \mu\text{m}$), this vortex ring will grow and destroy the whole vortex sheet. It is known that in superfluid $^3\text{He-B}$ the hard-core vortices of similar size are produced by neutron irradiation²¹. So we tried to make a hole in the vortex sheet in a similar way. However, irradiation by neutrons and by γ -quanta for several hours could not destroy the vortex sheet.

XII. CYLINDRICAL VORTEX SHEETS AS MULTIPLY QUANTIZED VORTICES

There are many possible equilibrium configurations of the rotating chiral superfluid $^3\text{He-A}$, which obey the solid body rotation of the liquid on a macroscopic scale. Practically all of them (including the array of vortex-skyrmions) are metastable. But if they are somehow created, they live practically forever. The main problem is to find the proper way for the preparation of particular configurations. There are many topological objects, which still avoided observation, because the scenarios for their creation have not been found. Among them are the half-quantum vortex and multiply quantized vortices.

The vortex sheet provides the possibility for the construction of multiply quantized vortices²². The closed vortex sheet with N merons represents the N -quantum

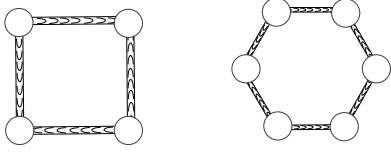


FIG. 12: Multiple vortices. Closed vortex sheets represent N -quantum vortices. Vortex sheets with $N = 4$ and $N = 6$ merons are illustrated. The radius of the N -quantum vortex is determined by the balance of forces: the repulsive interaction between the vortex-merons is compensated by the attraction due to surface tension of the soliton, see Eq.(7).

vortex. Since the $N = 2$ vortex is the known vortex skyrmion, and the odd number of merons in the closed vortex sheet is prohibited by topology, the multiply quantized vortices start with $N = 4$, see Fig. 12.

For large $N \gg 1$, the multiply quantized vortex is the cylindrical vortex sheet. Its radius r_N is obtained by minimization of the superflow energy outside the vortex + the energy of the soliton wall:

$$E_N = \pi \rho_s \frac{\hbar^2}{4m^2} N^2 \ln \frac{R}{r_N} + 2\pi \sigma r_N. \quad (5)$$

Here R is the radius of the cell. Minimization gives

$$r_N = N^2 \frac{\hbar^2 \rho_s}{8m^2 \sigma}. \quad (6)$$

For small N (but for $N > 3$) the cylinder should be substituted by the polyhedron – the N -gonal prism, Fig. 12. The radius of the prism is determined by the balance of forces: the repulsive interaction between vortices is compensated by the attraction due to surface tension of the soliton:

$$r_N = \frac{\pi(N-1)}{\sin(\pi/N)} \frac{\hbar^2 \rho_s}{8m^2 \sigma}. \quad (7)$$

Within the order of magnitude, Eqs.(6) and (7) give also the correct estimate for the core size of the skyrmion in Fig. 3, which consists of $N = 2$ merons.

XIII. MULTIPLE SHEETS

Though the array of small cylindrical sheets is energetically more favorable than the folded vortex sheet, we

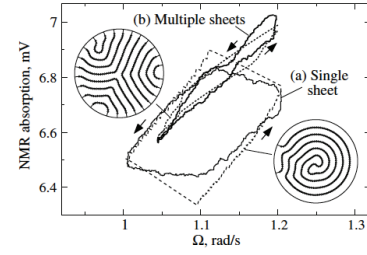


FIG. 13: Selection of rotating states by fast dynamics. *center*: The hysteresis loop in the state with the multiple vortex sheets is narrow compared to that in the state with a single folded sheet. In other words, the multiple sheets have much faster dynamics than the folded sheet. That is why the multiple sheets are better adjusted to the rotation, if the rotation is accompanied by rapid oscillations. *left insert*: numerical simulations for the configuration with multiple sheet. *right insert*: numerical simulations for the configuration with adiabatically grown folded sheet.

failed to produce them. Probably for that it is necessary to construct the proper disturbance on the container wall, which makes the creation of the cylindrical walls easier than the creation of skyrmions and of the vortex sheets connected to the wall.

Instead the way was found of how to split the folded vortex sheet into several pieces, which are connected to the side wall of container. The splitting occurs when the original single sheet is subjected to a high-frequency modulation with large amplitude²³, see Fig. 13. The obtained structure is determined by dynamics of merons. The narrow hysteresis loop in Fig. 13 corresponds to multiple sheets, which are formed after modulation $\Omega(t) = (1.2 + 0.4 \sin(\omega t))$ rad/s, with $2\pi/\omega = 10$ s. The response of the short sheets is faster than that of the folded sheet, since with the radial alignment of the sheets it is easier for merons to enter and escape the soliton during the fast modulation of angular velocity.

XIV. VORTEX SHEET AT AB INTERFACE

A crucial property of ^3He superfluids is the existence of the several length scales. In particular, the core size of a skyrmion in $^3\text{He-A}$ is 10^3 times larger than the core size of quantized vortices in $^3\text{He-B}$. The sharp (hard-core) vortices are not easily created: the critical velocity of the vortex nucleation under rotation is inversely proportional to the core radius²⁴. As a result one can prepare the state in the rotating cryostat, in which the A-phase skyrmion lattice simulates the macroscopic solid body rotation of

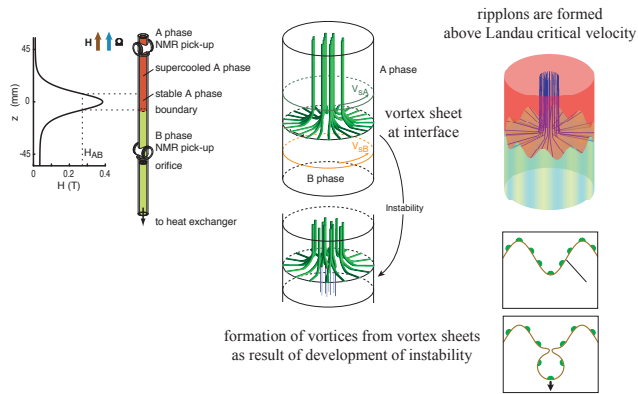


FIG. 14: Vortex sheet at the interface between rotating $^3\text{He-A}$ and the vortex-free $^3\text{He-B}$. (*left*): Experimental cell. The enhanced magnetic field at $z = 0$ prohibits propagation of the B-phase into the upper part of the cell. (*center top*): Vortex-full A-phase is separated from the vortex-free B-phase by the vortex sheet, which is concentrated at the AB interface. That is why the interface serves as tangential velocity discontinuity. (*right top*): When the velocity jump across the interface reaches the critical value, ripples are formed (analogous of the wind-generated surface waves). (*right bottom*): The development of the instability leads to the formation of the droplet of the vortex sheet inside the B-phase. Such sheet is unstable to formation of the quantized B-phase vortices (*center bottom*).

superfluid, while the B-phase is still in the static vortex-free state, which is called the Landau state. The A-phase vortex-skyrmions cannot penetrate from the A- to the B-phase, so they form a surface vortex sheet at the phase boundary²⁵, Fig. 14 *center top*. This sheet separates two superfluids moving with respect to each other. Near the boundary of the container the jump in the tangential velocity reaches $|v_A - v_B| = \Omega R$. This arrangement brings a lot of interesting physics.

(1) If the velocity difference $|v_A - v_B|$ exceeds the critical value, the interface experiences the instability towards the generation of the surface waves – ripples (analogous of the capillary-gravitational waves in conventional liquids), Fig. 14 *top right*. The onset of the analog of the Kelvin-Helmholtz instability is marked by the appearance of the vortex lines in $^3\text{He-B}$ which are detected in NMR measurements²⁶. At the non-linear stage of the instability the droplet of the vortex sheet is formed, Fig. 14 *right bottom*. It propagates into the B-phase, where it is unstable towards quantized vortices, Fig. 14 *center bottom*. This allowed us to measure the value of the critical velocity and compare it with the theory.

It appeared that the measured threshold of the instability is lower than that for the classical Kelvin-Helmholtz instability, and instead it satisfies the Landau critical velocity for the radiation of ripples, see details in²⁷ and in Chapter 27 of the book¹⁴. In the shallow water limit this corresponds to the Zel’dovich–Starobinsky

effect of radiation of the electromagnetic waves by rotating black holes (Chapter 31 in Ref.¹⁴).

(2) Formation of the B-phase vortices due to the instability of the surface vortex sheet allows us to use this phenomenon as the working tool for injection of vortices into the vortex-free B-phase under rotation. The injection of few vortices into superfluid in its metastable vortex-free Landau state revealed the new phenomenon in quantum turbulence²⁸. The NMR measurements after injection demonstrated the sharp transition to turbulence. At temperature above $0.60 T_c$ (where T_c is the transition temperature for superfluidity) the flow of superfluid is regular (laminar): the injected vortices from a small cluster in the center of the cell, Fig. 14 *center bottom*). However, below this temperature the turbulent behaviour is observed: vortices are multiplied in the turbulent regime and fill the whole cell.

Surprisingly, the observed sharp transition to turbulence is insensitive to the fluid velocity. This is in a striking contrast to classical turbulence regulated by the Reynolds number, which is proportional to the velocity of the liquid. The quantum superfluid turbulence is controlled by an intrinsic parameter of the superfluid: the Kopnin number Ko , which is the ratio of the reactive and dissipative parameters in the equations for superfluid hydrodynamics.

In the Fermi superfluids, such as superfluid ^3He and superconductors, the Kopnin number $Ko \sim \omega_0 \tau$, where ω_0 is the minigap – the distance between the levels of Andreev-Majorana fermions in the core of the vortex – and τ is their lifetime. For $Ko < 1$ the effect of chiral anomaly (spectral flow) provides the momentum exchange between vortices and the normal component of the liquid. In this regime dissipation is dominating, and the flow of the superfluid component is laminar. For $Ko > 1$ the effect of the inertial term is dominating, and the laminar flow becomes unstable towards turbulence.

XV. CONCLUSION

The vortex sheet structure of rotating superfluid has been calculated by Landau and Lifshitz in 1955. In 1995, i.e. 40 years later, it was experimentally demonstrated that for the complicated superfluids with the multi-component order parameter this concept was instrumental. The Landau-Lifshitz vortex sheet proved to be an important physical object with nontrivial topology and with many physical applications.

Acknowledgements

This work has been supported in part by the Academy of Finland (project no. 250280), and by the facilities of the Cryohall infrastructure of Aalto University.

- ¹ R.P. Feynman Application of quantum mechanics to liquid helium, in: *Progress in Low Temperature Physics* **1**, ed. C. J. Gorter, North-Holland, Amsterdam, pp. 17–53 (1955).
- ² L.D. Landau and E.M. Lifshitz, On the rotation of liquid helium, *Doklady Akademii Nauk SSSR* **100**, 669–672 (1955).
- ³ L. Onsager (unpublished), see F. London, *Superfluids*, Vol II (Wiley, New York), p 151.
- ⁴ H. London, in *Report of Intern. Conf. on Fund. Particles and Low Temp.*, Vol II, (Physical Society, London, 1946), p. 48.
- ⁵ V. L. Ginzburg, The surface energy associated with a tangential velocity discontinuity in Helium II, *ZhETF* **29**, 244–246 (1955); [*Sov. Phys. JETP* **2**, 170–172 (1956)].
- ⁶ I.M. Lifshitz and M.I. Kaganov, The effective density of rotating liquid Helium II, *ZhETF* **29**, 257–258 (1955); [*Sov. Phys. JETP* **2**, 172–174 (1956)].
- ⁷ Ü. Parts, M. Krusius, J.H. Koivuniemi, V.M.H. Ruutu, E.V. Thuneberg, G.E. Volovik, "Bragg reflection from the vortex-sheet planes in rotating $^3\text{He-A}$ ", *Pisma ZhETF* **59**, 816–820 (1994) [*JETP Lett.* **59**, 851–856 (1994)].
- ⁸ D. Vollhardt and P. Wölfle, *The superfluid phases of helium 3*, Taylor and Francis, London (1990).
- ⁹ T. Skyrme, A unified field theory of mesons and baryons, *Nucl. Phys.* **31**, 556–569 (1962).
- ¹⁰ N.D. Mermin and T.-L. Ho, Circulation and angular momentum in the A phase of superfluid helium-3, *Phys. Rev. Lett.* **36**, 594 (1976).
- ¹¹ H.K. Seppälä, P.J. Hakonen, M. Krusius, T. Ohmi, M.M. Salomaa, J.T. Simola, and G.E. Volovik, Continuous vortices with broken symmetry in rotating superfluid $^3\text{He-A}$, *Phys. Rev. Lett.* **52**, 1802–1805 (1984).
- ¹² S. Mühlbauer, Skyrmion lattice in a chiral magnet, *Science* **323**, 915 (2009).
- ¹³ G.E. Volovik and V.P. Mineev, Linear and point singularities in superfluid ^3He , *Pis'ma ZETF* **24**, 605–608 [*JETP Lett.* **24**, 561–563 (1976)].
- ¹⁴ G.E. Volovik, *The Universe in a Helium Droplet*, Clarendon Press, Oxford (2003)
- ¹⁵ L.M. Dedukh, B.I. Nikitenko and E.B. Sonin, Dynamics of Bloch lines in a domain wall, *Uspekhi Fiz. Nauk* **145**, 158–160 (1985) [*Sov. Phys. Uspekhi* **28**, 100–101 (1985)].
- ¹⁶ Ü. Parts, E.V. Thuneberg, G.E. Volovik, J.H. Koivuniemi, V.M.H. Ruutu, M. Heinilä, J.M. Karimäki, and M. Krusius, "Vortex sheet in rotating superfluid $^3\text{He-A}$ ", *Phys. Rev. Lett.* **72**, 3839–3842 (1994).
- ¹⁷ V.B. Eltsov, R. Blaauwgeers, M. Krusius, J.J. Ruohio, and R. Schanen, Dynamic response of the equilibrium vortex sheet in rotating $^3\text{He-A}$, *Physica B* **284–288**, 252 (2000).
- ¹⁸ M. Heinilä and G.E. Volovik, "Bifurcations in the growth process of a vortex sheet in rotating superfluid", *Physica, B* **210**, 300–310 (1995).
- ¹⁹ E.V. Thuneberg, "Introduction to the vortex sheet in superfluid $^3\text{He-A}$ ", *Physica, B* **210**, 287–299 (1995).
- ²⁰ M.M. Salomaa, G.E. Volovik, "Quantized Vortices in superfluid ^3He ," *Rev. Mod. Phys.* **59**, 533–613 (1987).
- ²¹ V.M.H. Ruutu, V.B. Eltsov, A.J. Gill, T.W.B. Kibble, M. Krusius, Yu.G. Makhlin, B. Placais, G.E. Volovik, Wen Xu, Vortex formation in neutron-irradiated superfluid ^3He as an analogue of cosmological defect formation, *Nature*, **382** 334–336 (1996).
- ²² G.E. Volovik and M. Krusius, "Superfluidity and quantized vortices in anisotropic $^3\text{He-A}$ ", in *Russain, Priroda* **4**, 56–69 (1994).
- ²³ V.B. Eltsov, R. Blaauwgeers, N.B. Kopnin, M. Krusius, J.J. Ruohio, R. Schanen, and E.V. Thuneberg, Transitions from vortex lines to sheets: interplay of topology and dynamics in an anisotropic superfluid, *Phys. Rev. Lett.* **88**, 65301 (2002).
- ²⁴ Ü. Parts, V.M.H. Ruutu, J.H. Koivuniemi, Yu. N. Bunkov, V.V. Dmitriev, M. Fogelström, M. Huenber, Y. Kondo, N.B. Kopnin, J.S. Korhonen, M. Krusius, O.V. Lounasmaa, P.I. Soininen, G.E. Volovik, "Single-vortex nucleation in rotating superfluid $^3\text{He-B}$ ", *Europhys. Lett.* **31**, 449–454 (1995).
- ²⁵ R. Hänninen, R. Blaauwgeers, V.B. Eltsov, A.P. Finne, M. Krusius, E.V. Thuneberg, G.E. Volovik, "Structure of surface vortex sheet between two rotating ^3He superfluids", *Phys. Rev. Lett.* **90**, 225301 (2003).
- ²⁶ R. Blaauwgeers, V. B. Eltsov, G. Eska, A.P. Finne, R.P. Haley, M. Krusius, J.J. Ruohio, L. Skrbek, and G. E. Volovik, "Shear flow and Kelvin-Helmholtz instability in superfluids", *Phys. Rev. Lett.* **89**, 155301 (2002).
- ²⁷ G.E. Volovik, "On Kelvin-Helmholtz instability in superfluids", *Pisma ZhETF* **75**, 491–495 (2002); *JETP Lett.* **75**, 418–422 (2002)
- ²⁸ A.P. Finne, T. Araki, R. Blaauwgeers, V.B. Eltsov, N.B. Kopnin, M. Krusius, L. Skrbek, M. Tsubota, and G.E. Volovik, "An intrinsic velocity-independent criterion for superfluid turbulence", *Nature* **424**, 1022–1025 (2003).